ORIGINAL RESEARCH

Molecular docking-based virtual screening, molecular dynamic simulation, and 3-D QSAR modeling of some pyrazolopyrimidine analogs as potent anti-filarial agents

Fabian Audu Ugbe[1] · Gideon Adamu Shallangwa[1] · Adamu Uzairu[1] · Ibrahim Abdulkadir[1]

Abstract

Lymphatic filariasis and onchocerciasis are common filarial diseases caused by filarial worms, which co-habit symbiotically with the *Wolbachia* organism. One good treatment method seeks *Wolbachia* as a drug target. Here, a computer-aided molecular docking screening and 3-D QSAR modeling were conducted on a series of Fifty-two (52) pyrazolopyrimidine derivatives against four *Wolbachia* receptors, including a pharmacokinetics study and Molecular Dynamic (MD) investigation, to find a more potent anti-filarial drug. The DFT approach (B3LYP with 6-31G** option) was used for the structural optimization. Five ligand-protein interaction pairs with the highest binding affinities were identified in the order; 23_7ESX (-10.2 kcal/mol) > 14_6EEZ ($-$ 9.0) > 29_3F4R ($-$ 8.0) > 26_6W9O ($-$ 7.7) $\approx$ doxycycline_7ESX ($-$ 7.7), with good pharmacological interaction profiles. The built 3-D QSAR model satisfied the requirement of a good model with $R^2 = 0.9425$, $Q^2_{LOO} = 0.5019$, SDEC $= 0.1446$, and F test $= 98.282$. The selected molecules (**14, 23, 26**, and **29**) perfectly obeyed Lipinski's RO5 for oral bio-availability, and showed excellent ADMET properties, except **14** with positive AMES toxicity. The result of the MD simulation showed the great stability associated with the binding of **23** onto 7ESX's binding pocket with an estimated binding free energy (MM/GBSA) of $-$ 60.6552 kcal/mol. Therefore, **23** could be recommended as a potential anti-filarial drug molecule, and/or template for the design of more prominent inhibitors.

Keywords Filarial diseases · *Wolbachia* · Pyrazolopyrimidine · Molecular docking · 3-D QSAR · Pharmacokinetics · Molecular dynamics

Abbreviations

ADMET	Absorption, distribution, metabolism, excretion, and toxicity
ALA	Alanine
ARG	Arginine
ASN	Asparagine
ASP	Aspartic acid
B3LYP	Becke's three-parameter read-Yang-Parr hybrid
BBB	Blood brain barrier
CHARMM	Chemistry at Harvard macromolecular mechanics
CidA	Cytoplasmic incompatibility factor A
CNS	Central nervous system
CoMFA	Molecular field analysis
CPU	Central processing unit
CYP-34A/CYP-2D6	Cytochrome p450 isoforms
DFT	Density functional theory
EC_{50}	Half-maximal inhibitory concentration
ESOL	Estimated solubility
F test	Fischer's statistics
GLU	Glutamic acid
HBA	Hydrogen bond acceptor
HBD	Hydrogen bond donor
HIA	Human intestinal absorption
HIS	Histidine
ILE	Isoleucine
LEU	Leucine
LMO	Leave many out

✉ Fabian Audu Ugbe
ugbefabianaudu@gmail.com

1   Department of Chemistry, Faculty of Physical Sciences, Ahmadu Bello University, P.M.B. 1044, Zaria, Kaduna State, Nigeria

LogBB	Logarithmic ratio of brain to plasma drug concentration
LogPS	Blood-brain permeability-surface area product
LOO	Leave one out
LTO	Leave two out
LF	Lymphatic filariasis
LYS	Lysine
MD	Molecular dynamics
MDA	Mass drug administration
MIFs	Molecular interaction fields
MMFF	Molecular mechanics force field
MM/GBSA	Molecular mechanics generalized born surface area
MRTD	Maximum recommended tolerated dose
MW	Molecular weight
NAMD	Nano-scale molecular dynamics
NTD	Neglected tropical diseases
O3A	Open3D align
PC	Principal component
PDB	Protein data bank
pEC_{50}	Negative log of EC_{50}
PHE	Phenylalanine
PRO	Proline
QSAR	Quantitative structure activity relationship
Rg	Radius of gyration
RAM	Random access memory
RMSD	Root-mean-square deviation
RMSF	Root-mean-square fluctuation
RO5	Rule of five
SA	Synthetic accessibility
SDEC	Standard error of correlation
SDEP	Standard error of prediction
SEE	Standard error of estimation
SER	Serine
SASA	Solvent accessible surface area
TPSA	Topological polar surface area
TRP	Tryptophan
TYR	Tyrosine
UVE-PLS	Un-informative variable elimination-partial least square
VAL	Valine
VMD	Visual molecular dynamics

Introduction

Lymphatic Filariasis (LF) also known as elephantiasis and Onchocerciasis (river blindness) are common Neglected Tropical Diseases (NTD), which are caused by some parasitic nematode worms (Sightsavers 2013). LF is caused by filarial worms like *Wuchereria bancrofti*, *Brugia timori* and *Brugia malayi*, which are been transmitted by mosquitoes, while *Onchocerca volvulus* is the causative agent for onchocerciasis, which is transmitted from one person to another by blood-feeding black flies (Bakowski et al. 2019). Elephantiasis alone is responsible for not less than 2.8 million disabilities globally (Jacobs et al. 2019). The global program intended to eliminate these filarial diseases started far back through the Mass Drug Administration (MDA) of anti-filarial such as ivermectin, albendazole, and diethylcarbamazine, either as a dual (annual to bi-annual) or as triple-drug (once every 3 years) treatment (Jacobs et al. 2019; Carter et al. 2020). However, it became unlikely that the MDA regimen will be adequate to eliminate these filarial diseases in all endemic areas, majorly due to their inability to kill the macrofilariae (Lakshmi et al. 2010). Given the current scenario, therefore, a macrofilaricidal agent is required to kill worms to reduce both diseases' elimination time frames (Sashidhara et al. 2014).

Fortunately, one unique characteristic of these filarial worms is their symbiotic co-existence with a known bacterium referred to as *Wolbachia* (Slatko et al. 2010). In the search for new anti-filarial drugs, some researchers have chosen the option of targeting *Wolbachia*, which past research has shown that its elimination from the host filarial nematodes leads to antifilarial effects with the reduction of adult worm's lifespan (Bouchery et al. 2013; McGillan 2017). Although the anti-bacteria drug, doxycycline has been used clinically for the treatment of filarial diseases over the years, the treatment method is not efficient enough for use in mass administration including requirements for long treatment periods (4–6 weeks) as well as contraindications in pregnancy and children (McGillan 2017). Therefore, advances in the development of new anti-*Wolbachia* agents with short treatment periods and reduced complications are necessary.

Some compounds of the pyrazolopyrimidine class were earlier reported to show a variety of bioactivities such as anti-viral agents, anti-malarial, anti-depressants, anti-tuberculosis, and kinase inhibitors (McGillan et al. 2021; Ugbe et al. 2022a). However, certain side effects have been associated with most of the drugs in this class such as hypnotic and/or anxiolytic effects. To further explore the anti-filarial effect of the pyrazolopyrimidine compounds, McGillan (2017) synthesized several pyrazolopyrimidine derivatives and reported their inhibitory activities against *Wolbachia* infected insect cells (Aedes albopictus, C6/36). Notable targets of *Wolbachia pipientis* include Oxidoreductase α-DsbA1 (PDB ID: 3F4R), OTU deubiquitinase (6W9O), thiol-disulfide exchange protein alpha-DsbA2 (6EEZ), and Cytoplasmic incompatibility factor CidA (7ESX) amongst others.

Computer-aided drug design plays a crucial role in the discovery of new drug molecules in pharmaceutical design,

drug metabolism, and medicinal chemistry. It saves time, and cost and tends to be highly effective for the evaluation of a large virtual database of chemical compounds (Adeniji et al. 2020). Molecular docking simulation computer-aided screening method which probes the binding of ligands in the active sites of the protein target using a valid docking tool (Ibrahim et al. 2020). Pharmacokinetics analysis on the other hand is important in the pre-clinical study of new drug compounds to ascertain how such drug compounds affect the living organism when administered. Some of the most important pharmacokinetic properties to be determined during pre-clinical testing include Absorption, Distribution, Metabolism, Excretion, and Toxicity (ADMET) (Lawal et al. 2021; Ibrahim et al. 2021). Physico-chemical properties such as molecular weight, Topological Polar Surface Area (TPSA), lipophilicity, hydrogen bond donors, and hydrogen bond acceptors amongst others are necessary to predict a drug's likelihood of being orally bioavailable (Lipinski et al. 2001). This work focuses on the virtual molecular docking screening of a series of Fifty-two (52) pyrazolopyrimidine derivatives against Four (4) *Wolbachia* targets, 3-D QSAR modeling, Molecular Dynamics (MD) simulation, and prediction of pharmacokinetic properties of some selected analogs, to find a more potent drug molecule which would be suitable for the treatment of filarial diseases.

Materials and methods

Data acquisition

A series of Fifty-two (52) pyrazolopyrimidine derivatives with reported bioactivities (EC_{50} in nM) against *Wolbachia*-infected insect cells (Aedes albopictus, C6/36), were sourced from the literature (McGillan 2017). The various bioactivity (EC_{50}) values were separately converted to pEC_{50} using Eq. (1) (Ugbe et al. 2022a). The molecular structures of the various pyrazolopyrimidine derivatives were shown in Online Resource 1.

$$pEC_{50} = -log_{10}\left(EC_{50} \times 10^{-9}\right) \qquad (1)$$

Ligand preparation

The molecular structures of all the compounds were drawn using the ChemDraw Ultra, saved as MDL molfile format, and thereafter imported separately onto the Spartan '14 Graphical User Interface while enabling the auto conversion of 2-D models to 3-D. The imported molecules were initially subjected to energy minimization and then saved in Spartan file format. The resulting structures were then fully optimized first by using Molecular Mechanics Force

Field (MMFF) and thereafter Density Functional Theory (DFT) with Becke's three-parameter read-Yang-Parr hybrid (B3LYP) option and utilizing the 6-31G basis set. The optimized structures were then saved as PDB and SD file formats for subsequent use in molecular docking and 3-D QSAR studies respectively (Wang et al. 2020; Ugbe et al. 2021).

Preparation of the protein receptors

The crystal structures of Four (4) *Wolbachia* target proteins (PDB codes: 3F4R, 6EEZ, 6W9O, and 7ESX) were retrieved from the RCSB Protein Data Bank in PDB file format, and then prepared separately using the Molegro virtual docker by eliminating water molecules, cofactors and co-crystallized ligands contained within the protein structures (Ugbe et al. 2022b). The various receptors used in the virtual docking screening were described in Table 1.

Molecular docking-based screening

Molecular docking investigation was performed separately between the Four (4) different receptors of *Wolbachia pipientis* and all 52 compounds, including the reference drug (Doxycycline) using the Auto Dock Vina of PyRx v software tool (Ugbe et al. 2021). The screening was conducted to ascertain the most active pyrazolopyrimidine compounds against the various protein targets. PyRx calculates the binding affinities of the receptor-ligand interactions which are necessary to describe how fit the molecules bind to the target protein. A more negative binding affinity will indicate a greater chance of the potential drug molecule to initiate protein biochemical action/reaction (Kumar et al. 2016).

Evaluation of pharmacokinetic properties

Predicting pharmacokinetics properties plays a critical role in the early stage of drug discovery. This is because only molecules which demonstrate good ADMET and drug-likeness properties reach the pre-clinical research phase (Ugbe et al. 2021). Therefore, Four (4) pyrazolopyrimidine analogs (**14,**

Table 1 Description of enzymes used for the docking screening

S. No	Enzyme	Organism	PDB ID	Resolution (Å)
1	Alpha-DsbA1	*Wolbachia*	3F4R	1.60
2	Alpha-DsbA2	*Wolbachia*	6EEZ	2.25
3	OTU deubiquitinase	*Wolbachia*	6W9O	1.47
4	Cytoplasmic incompatibility factor CidA	*Wolbachia*	7ESX	1.80

PDB ID – 3F4R, 6EEZ, 6W9O, 7ESX

23, **26**, and **29**) having the highest binding scores with 6EEZ, 7ESX, 6W9O, and 3F4R respectively were subjected to drug-likeness and ADMET tests using two online web servers; http://www.swissadme.ch/index.php and http://biosig.unimelb.edu.au/pkcsm respectively. Lipinski's rule of five (RO5) also called the Pfizer rule is a well-established provision for determining the oral bioavailability of a given compound (Lipinski et al. 2001; Lawal et al. 2021). Consequently, these analogs were subjected to the RO5 criterion to ascertain their oral bioavailability.

Molecular dynamics simulation and MM/GBSA calculation

Molecular dynamics (MD) simulation of **7ESX_23** complex was performed using the combined approach of Chemistry at Harvard Macromolecular Mechanics (CHARMM) force field, Nano-scale Molecular Dynamics (NAMD), and Visual Molecular Dynamics (VMD). The CHARMM-GUI, an established web-based platform that utilizes the CHARMM force field, was used to generate the input files for the simulation by NAMD (Lee et al. 2016). The periodic boundary condition was utilized while fitting the system into a cubic water box for solvation. The protein was solvated and neutralized explicitly in an aqueous solution of 0.10 M concentration of potassium chloride salt (Edache et al. 2022). To stabilize the complex structure and to ensure steric clashes will not result, energy minimization was performed. The resulting system of ions and solvent was then equilibrated to stabilize the system at a temperature chosen for the simulation (310.15 K) at a constant number of particles, volume, and temperature (NVT ensemble), and to stabilize the pressure by keeping the number of particles, pressure, and temperature (NPT ensemble) constant using 100ps time frame (Muniba 2019). MD was then performed on the resulting system for 1ns (500,000 steps), while the results were visualized using VMD and the Biovia discovery studio, all on an HP laptop computer; Processor (Intel(R) Core(TM) i5-4210U CPU @ 1.70 GHz 2.40 GHz), Installed RAM (8.00 GB), System type (64-bit operating system, x64-based processor), Edition (Windows 10 Home Single Language), Version 21H2. A similar procedure was described elsewhere (Edache et al. 2022). Additionally, MolAICal software was used to compute the ligand-binding affinity by Molecular Mechanics Generalized Born Surface Area (MM/GBSA) method based on the resulting MD log files obtained with NAMD (Bai et al. 2020). MM/GBSA is estimated using Eqs. (2)–(4) (Bai et al. 2020).

$$\Delta G_{bind} = \Delta H - T\Delta S \approx \Delta E_{MM} + \Delta G_{sol} - T\Delta S \tag{2}$$

$$\Delta E_{MM} = \Delta E_{internal} + \Delta E_{ele} + \Delta E_{vdw} \tag{3}$$

$$\Delta G_{sol} = \Delta G_{SA} + \Delta G_{GB} \tag{4}$$

Where, ΔE_{MM} and $-T\Delta S$ represent respectively the gas phase MM energy and conformational entropy. ΔE_{MM} contains electrostatic ΔE_{ele}, van der Waals energy ΔE_{vdw} and $\Delta E_{internal}$ of bond, angle, and dihedral energies. ΔG_{sol} is the solvation free energy equal to the sum of the nonelectrostatic solvation component ΔG_{SA} and electrostatic solvation energy ΔG_{GB}.

3 – D QSAR modeling

The alignment of molecular structures plays a critical role in 3D-QSAR modeling (Al-Attraqchi and Mordi 2022) as it strongly determines the predictive accuracy and statistical quality of any given 3D-QSAR model (ElMchichi et al. 2020). Different alignment methods have been reported previously such as atom-based, docking-based, pharmacophore-based, and co-crystallized conformer-based alignments amongst others (Zhang et al. 2020; Al-Attraqchi and Mordi 2022). In this study, the atom-based alignment was adopted using the Open3DAlign (O3A) tool. The atom-based method attempts to match the atoms of the various structures to be aligned with those of the template structure, based on the atom's properties such as the partial charge.

The aligned structures were used for building the 3-D QSAR model using the Open3DQSAR software (Zhang et al. 2020). The Comparative Molecular Field Analysis (CoMFA) which is concerned with steric and electrostatic fields' contributions was studied (ElMchichi et al. 2020). A dataset of 52 compounds was divided into a training set and a test set of 36 and 16 molecules respectively, i.e. percentage ratio of 70:30. The steric and electrostatic Molecular Interaction Fields (MIFs) analysis was carried out on the aligned compounds placed within a 3-D cubic lattice of grid size 1.5 Å and a 5.0 Å out gap (Tosco and Balle 2011). Variables pretreatment was carried out as follows; energy cut-off (30.0 kJ/mol), elimination of variables having constant or near-constant values, and standard deviation cut-off (level = 2.0) (Al-Attraqchi and Mordi 2022). The Un-informative Variable Elimination-Partial Least Square (UVE-PLS) was used to build the statistical model and for generating the steric and electrostatic contour plots (Edache et al. 2022). The resulting model was then cross-validated using the Leave-One-Out (LOO), Leave-Two-Out (LTO), and Leave-Many-Out (LMO). The steric and electrostatic contour maps were visualized on Maestro v. 12.3.

Results and discussion

Virtual docking screening

The results (binding affinities) of the docking simulation conducted between the Four (4) receptors of *Wolbachia*

Table 2 Summary of binding affinities of interactions between pyrazolopyrimidine derivatives and different *Wolbachia pipientis* receptors used for the target fishing

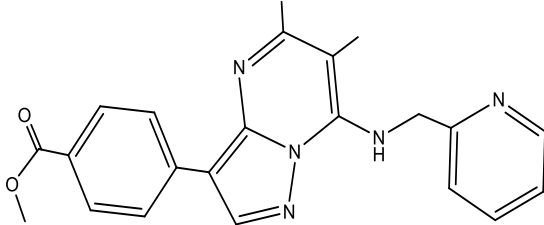| Comp ID	Protein-ligand binding affinities (kcal/mol)			
	3F4R	6EEZ	6W9O	7ESX
1	− 7.0	− 8.5	− 7.1	− 8.3
2	− 6.9	− 8.1	− 6.8	− 8.0
3	− 7.4	− 8.3	− 7.2	− 9.4
4	− 7.6	− 8.3	− 7.3	− 8.1
5	− 7.2	− 8.8	− 7.3	− 8.0
6	− 7.1	− 8.6	− 7.1	− 7.8
7	− 6.9	− 8.1	− 7.0	− 8.2
8	− 6.9	− 8.4	− 7.2	− 8.5
9	− 7.2	− 7.9	− 7.5	− 8.2
10	− 7.0	− 7.7	− 7.0	− 8.0
11	− 6.9	− 8.0	− 7.0	− 8.0
12	− 7.0	− 8.4	− 7.3	− 7.9
13	− 7.1	− 8.0	− 7.4	− 7.5
14	− 7.5	− 9.0	− 7.3	− 8.8
15	− 7.4	− 8.6	− 6.8	− 8.1
16	− 7.3	− 8.7	− 6.9	− 8.7
17	− 7.2	− 8.3	− 7.4	− 8.6
18	− 6.9	− 8.4	− 7.5	− 8.4
19	− 6.8	− 7.5	− 6.9	− 8.7
20	− 7.4	− 7.6	− 7.3	− 8.5
21	− 7.0	− 7.6	− 7.1	− 8.4
22	− 7.3	− 8.6	− 6.9	− 7.8
23	− 7.4	− 7.4	− 7.0	− 10.2
24	− 7.1	− 6.9	− 7.2	− 8.0
25	− 6.6	− 7.4	− 7.3	− 7.3
26	− 7.7	− 8.2	− 7.7	− 8.1
27	− 7.6	− 8.2	− 7.3	− 8.9
28	− 7.8	− 8.5	− 7.6	− 9.0
29	− 8.0	− 8.1	− 7.7	− 7.8
30	− 7.3	− 8.0	− 7.2	− 7.8
31	− 7.1	− 7.5	− 7.2	− 7.8
32	− 6.3	− 6.2	− 5.8	− 7.7
33	− 6.3	− 6.6	− 6.0	− 7.6
34	− 6.3	− 6.3	− 6.3	− 7.2
35	− 6.7	− 6.6	− 6.5	− 7.5
36	− 6.9	− 6.6	− 6.8	− 7.4
37	− 5.9	− 6.8	− 5.8	− 7.2
38	− 6.4	− 6.4	− 6.6	− 7.4
39	− 6.7	− 7.3	− 6.5	− 7.9
40	− 6.7	− 7.6	− 6.6	− 8.9
41	− 7.2	− 7.7	− 6.8	− 7.7
42	− 6.6	− 7.9	− 7.0	− 8.2
43	− 6.8	− 7.6	− 6.9	− 8.2
44	− 6.8	− 7.5	− 7.3	− 7.8
45	− 6.2	− 6.3	− 6.0	− 8.0
46	− 7.1	− 8.5	− 7.3	− 7.5
47	− 6.7	− 7.0	− 7.0	− 7.7

Table 2 (continued)
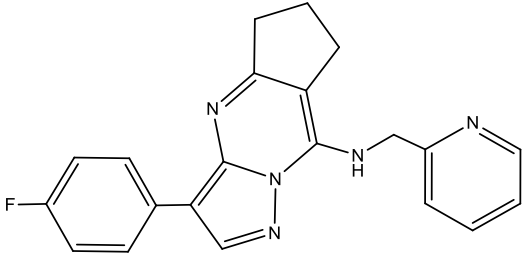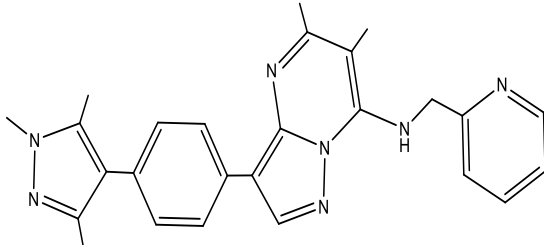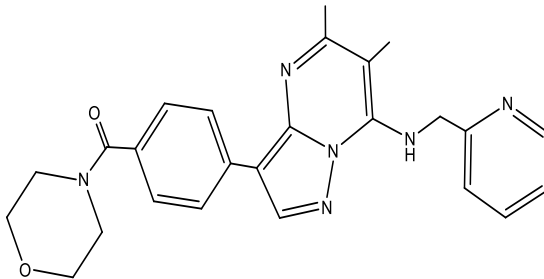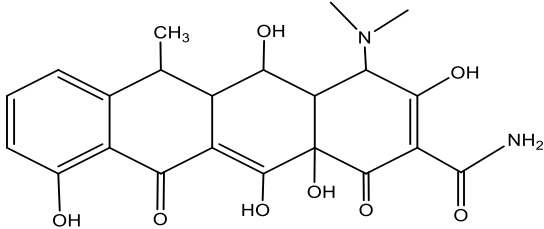
Comp ID	Protein-ligand binding affinities (kcal/mol)			
	3F4R	6EEZ	6W9O	7ESX
48	− 6.8	− 7.6	− 6.5	− 7.9
49	− 6.8	− 7.4	− 6.8	− 8.1
50	− 6.9	− 7.2	− 6.9	− 7.4
51	− 6.8	− 7.1	− 6.7	− 8.7
52	− 6.8	− 6.5	− 6.1	− 7.5
Ref	− 6.9	− 6.9	− 7.4	− 7.7

PDB ID – 3F4R, 6EEZ, 6W9O, 7ESX, *Ref* reference drug (Doxycycline)

pipientis and the various pyrazolopyrimidine derivatives, as well as the reference drug (Doxycycline), were reported in Table 2.. It can be observed from Table 2 that no particular ligand best interacted with all the studied receptors combined. That is, a ligand may bind very strongly with a given receptor but shows a weak interaction with another receptor. However, Four (4) ligand-protein interaction pairs with the greatest negative binding scores were identified in the order; compound **23** with 7ESX (-10.2 kcal/mol)> **14** with 6EEZ (− 9.0 kcal/mol)> **29** with 3F4R (− 8.0 kcal/mol) > **26** with 7ESX (− 7.7 kcal/mol). Also, no ligand-protein interaction pair involving the reference drug (Doxycycline) was identified that could compare with the identified interaction pairs, except doxycycline_7ESX complex with a binding score of − 7.7 kcal/mol equal to that of **26**_7ESX complex. Therefore, the virtual screening was effective and subsequent discussion shall be based on these more active molecules (Table 3).

The pharmacological interactions between the receptors' amino acid residues and the selected compounds (**14**, **23, 26**, and **29**) as well as the reference drug (Doxycycline) were summarized in Table 4, while the 2D and 3D views of the binding interactions as adapted from the Discovery Studio Visualizer were shown in Figs. 1, 2, 3, 4, and 5. This was to provide insight into the mode of binding of these ligands with the active sites of the various target proteins.These compounds were said to interact very adequately with the respective target receptors as shown by the presence of hydrogen bonding (H-bond), hydrophobic interactions, and in some cases electrostatic interactions. (Table 4). However, more interactions were visible from the binding profile of compound **23** with 7ESX, involving a total of Four (4) conventional H-bonds, One (1) π-donor H-bond, One (1) π-anion electrostatic interaction, and up to Eight (8) hydrophobic interactions. Four groups can be identified in the molecular structure of compounds 23 as pyridine, pyrimidine, pyrazole, and benzoate groups, all interacting significantly with the receptor's amino acid residues. The carbonyl group (C=O) oxygen of the benzoate group

Table 3 Molecular structures of some selected pyrazolopyrimidine analogs

Comp ID	Molecular structures
14	
23	
26	
29	
Doxycycline	

formed 2 H-bonds with LYS-232 at interaction distances of 2.68 and 2.91 Å. The remaining 2 conventional H-bonds were formed by GLU-188 with the pyridine group and the linker amine group at 2.01 Å and 3.05 Å respectively. Also, the π-donor H-bond was between ASN-77 and the pyrazole π-system at 2.96 Å. Visible were the π-anion interactions between the π-electrons systems of GLU-191 and the benzoate group at 4.06Å. Several hydrophobic interactions were formed including π- π T shaped with PHE-228 (5.22 Å), π-sigma with ARG-74 (3.57 Å), π-alkyl with TRP-37 at 5.39 Å, LEU-75 at 5.44 Å, and ARG-74 at 4.30 Å and 5.49Å, and alkyl interactions with ARG-36 and LEU-75 at distances of 4.95 Å and 4.64 Å respectively. It is important to note that no unfavorable interaction was seen in the **23_7ESX** binding interaction profile (Fig. 1). The complex involving the reference drug, **doxycycline_7ESX** on the other hand

Table 4 Predicted binding interaction profiles of **14**, **23**, **26**, **29**, and Doxycycline with the receptors

Complex	Binding affinity (kcal/mol)	Amino acid	Bond type	Interaction	Distance (Å)
7ESX_23	− 10.20	GLU-188	Hydrogen bond	Conventional hydrogen bond	2.01, 3.05
		LYS-232	Hydrogen bond	Conventional hydrogen bond	2.68, 2.91
		ASN-77	Hydrogen bond	π-donor hydrogen bond	2.96
		GLU-191	Electrostatic	π-anion	4.06
		PHE-228	Hydrophobic	π- π T shaped	5.22
		ARG-74	Hydrophobic	π-sigma	3.57
		TRP-37	Hydrophobic	π-alkyl	5.39
		LEU-75	Hydrophobic	π-alkyl	5.44
		ARG-74	Hydrophobic	π-alkyl	4.30, 5.49
		ARG-36	Hydrophobic	Alkyl	4.95
		LEU-75	Hydrophobic	Alkyl	4.64
6EEZ_14	− 9.00	LYS-155	Hydrogen bond	Conventional hydrogen bond	2.30, 2.57
		TYR-89	Hydrogen bond	Carbon hydrogen bond	2.99
		LYS-118	Hydrogen bond	Carbon hydrogen bond	3.49
		PHE-159	Hydrophobic	π- π stacked	3.85
		TYR-89	Hydrophobic	π- alkyl	5.47
3F4R_29	− 8.00	ASP-103	Hydrogen bond	Conventional hydrogen bond	2.94
		LYS-109	Hydrogen bond	Conventional hydrogen bond	2.41, 2.67
		ASP-103	Hydrogen bond	Carbon hydrogen bond	3.73
		ASN-106	Hydrophobic	π-sigma	3.97
		ALA-110	Hydrophobic	π-alkyl	4.63
		ALA-110	Hydrophobic	Alkyl	3.64
6W9O_26	− 7.70	GLU-81	Hydrogen bond	Carbon hydrogen bond	3.62
		ARG-131	Electrostatic	π-cation	3.61
		GLU-135	Electrostatic	π-anion	4.44
		PHE-82	Hydrophobic	π- π T shaped	4.71
		PRO-88	Hydrophobic	π-sigma	3.64
		TRP-90	Hydrophobic	π-alkyl	4.88
		PRO-88	Hydrophobic	π-alkyl	5.43
		PRO-88	Hydrophobic	Alkyl	4.25
		LYS-85	Hydrophobic	Alkyl	4.74
		LYS-85	Donor-donor	Unfavorable	2.01
7ESX_ Doxycycline	− 7.70	ILE-288	Hydrogen bond	Conventional hydrogen bond	2.03
		TYR-251	Hydrogen bond	Conventional hydrogen bond	2.56
		LEU-243	Hydrogen bond	Conventional hydrogen bond	2.67
		LYS-246	Hydrogen bond	Conventional hydrogen bond	2.09
		LYS-248	Hydrogen bond	Conventional hydrogen bond	2.03
		PHE-289	Hydrogen bond	Conventional hydrogen bond	2.81
		SER-290	Hydrogen bond	Carbon hydrogen bond	3.51
		LYS-287	Hydrogen bond	Carbon hydrogen bond	3.22
		SER-244	Hydrogen bond	Carbon hydrogen bond	3.03
		LYS-287	Hydrophobic	π-alkyl	5.50
		VAL-250	Donor-donor	Unfavorable	1.17

ALA alanine, *ARG* arginine, *ASN* asparagine, *ASP* aspartic acid, *GLU* glutamic acid, *ILE* isoleucine, *LEU* leucine, *LYS* lysine, *PHE* phenylalanine, *PRO* proline, *SER* serine, *TRP* tryptophan, *TYR* tyrosine, *VAL* valine
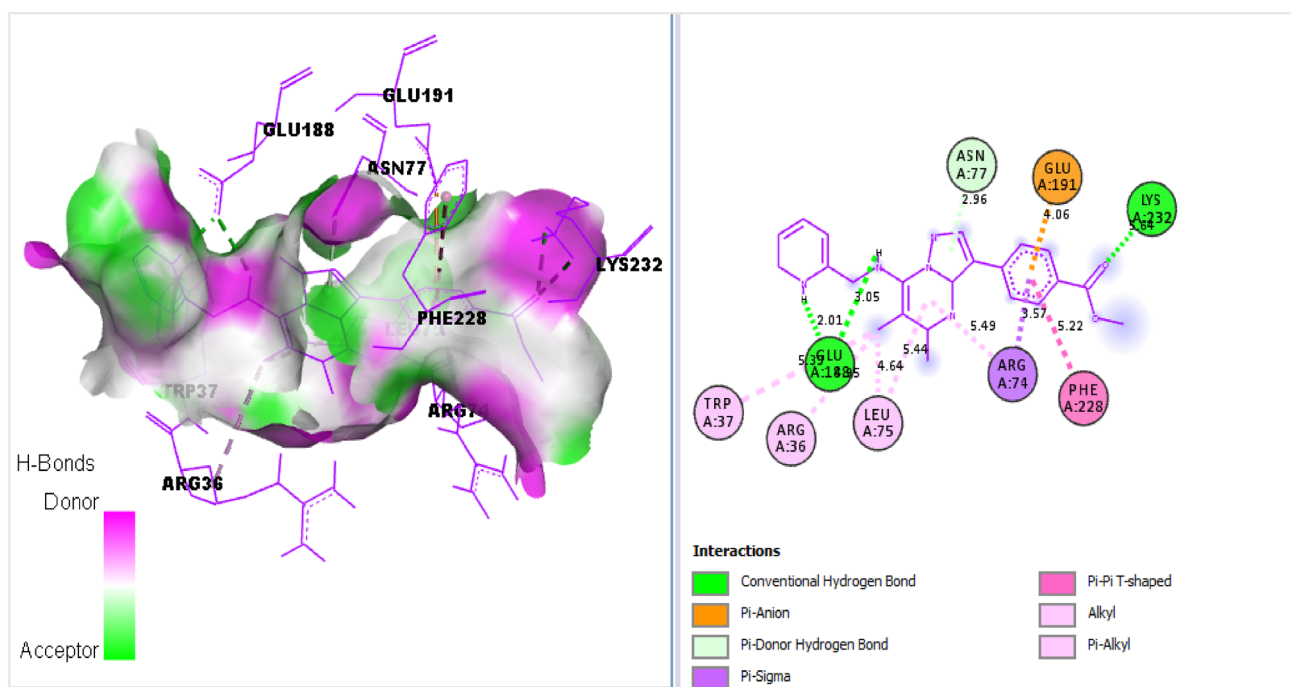
Fig. 1 Binding interaction between **23** and Cytoplasmic incompatibility factor CidA (PDB: 7ESX)

showed more H-bonding interactions than **23_7ESX**, consisting of a total of Six (6) conventional H-bonds and Three (3) Carbon-H-bonds. Only One (1) hydrophobic interaction was however visible. More so, an unfavorable donor-donor clash with VAL-250 was formed (Fig. 5). Therefore, compound **23** exhibited stronger and safer binding interactions with the Cytoplasmic incompatibility factor CidA than the reference drug (doxycycline)
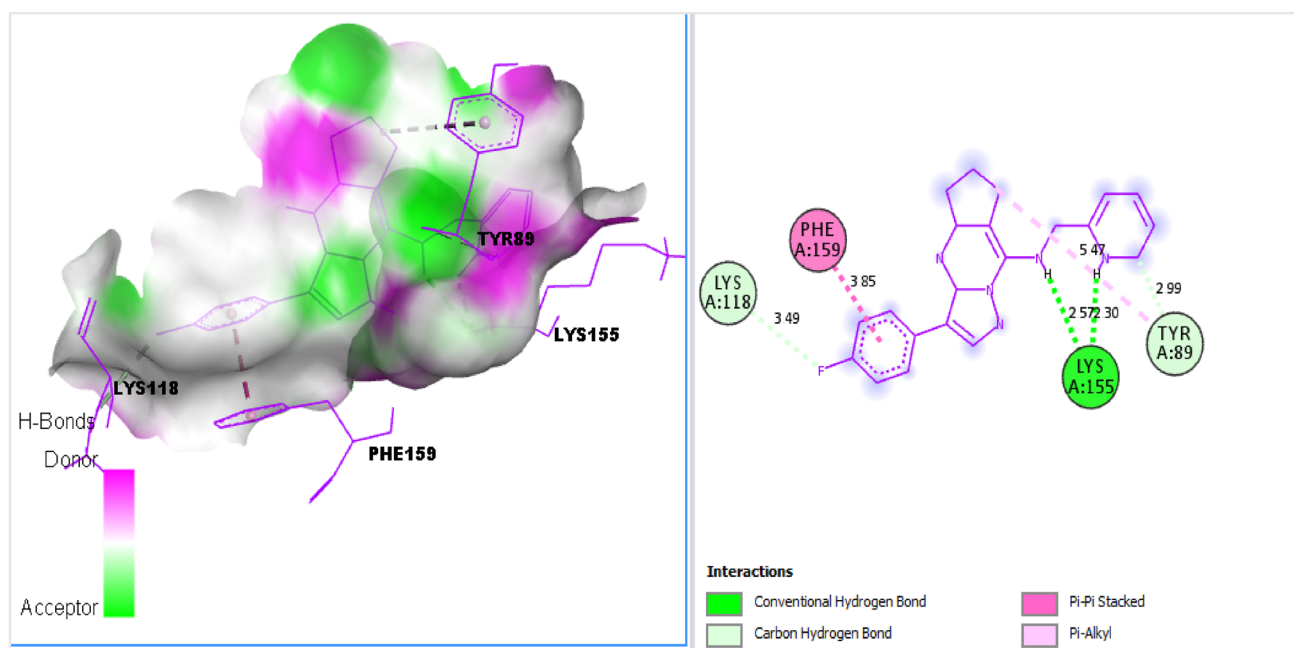
Fig. 2 Binding interaction between **14** and Alpha-DsbA2 (PDB: 6EEZ)
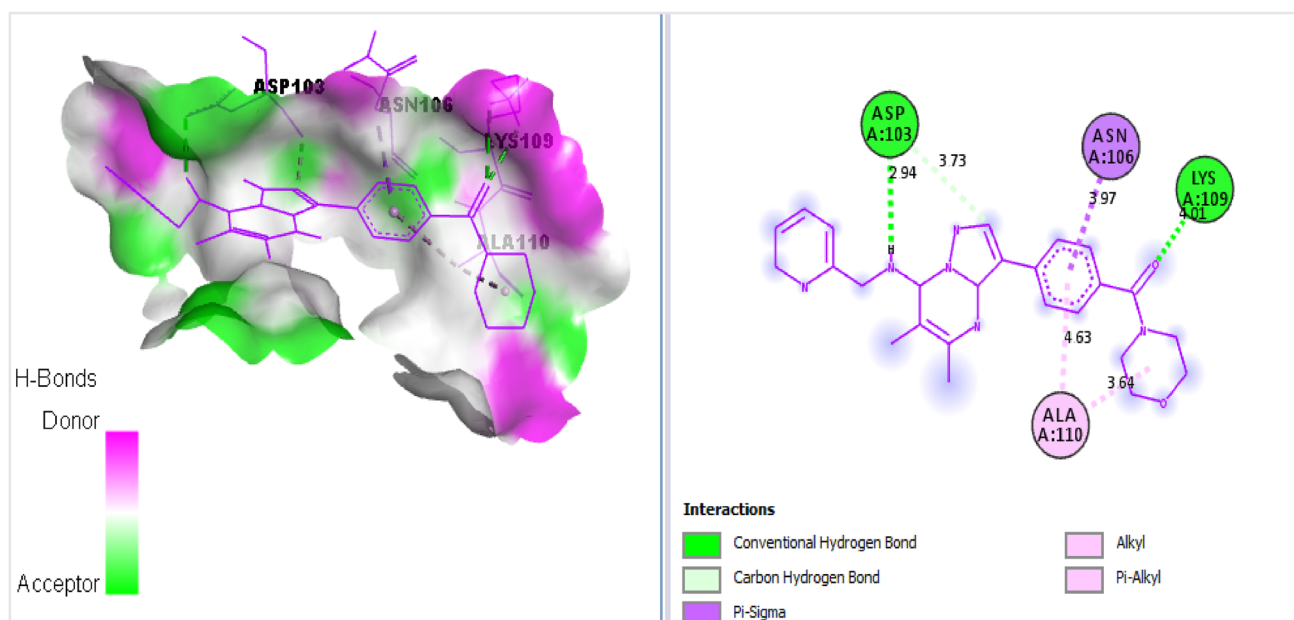
Fig. 3 Binding interaction between **29** and Alpha-DsbA1 (PDB: 3F4R)

Evaluation of pharmacokinetic properties

Drug-likeness analysis and ADMET study were conducted on the Four (4) compounds (**14**, **23**, **26**, and **29**) to ascertain their oral bioavailability. The results of both investigations were presented in Tables 5 and 6 respectively, while Fig. 6 shows their Boiled Egg's representation.

Lipinski's RO5 for oral-bioavailability has been widely applied in the discovery of new drug molecules (Ugbe et al. 2022b). It asserts that a drug molecule may likely
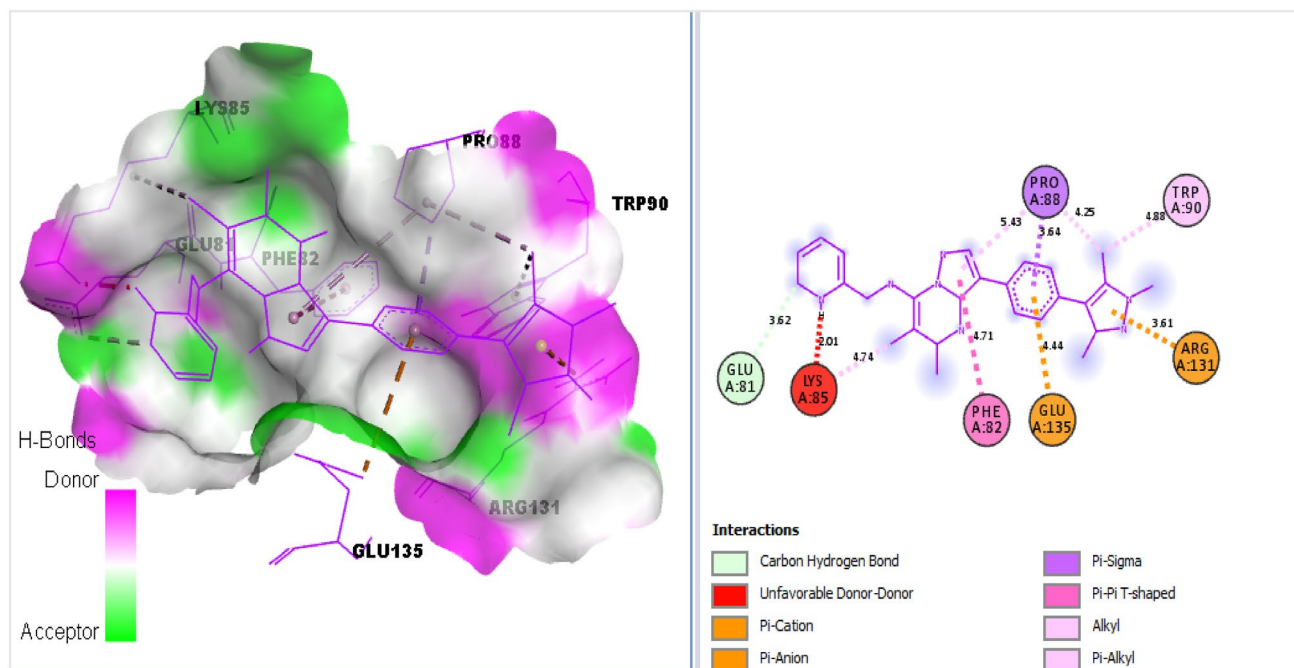
Fig. 4 Binding interaction between **26** and OTU deubiquitinase (PDB: 6W9O)
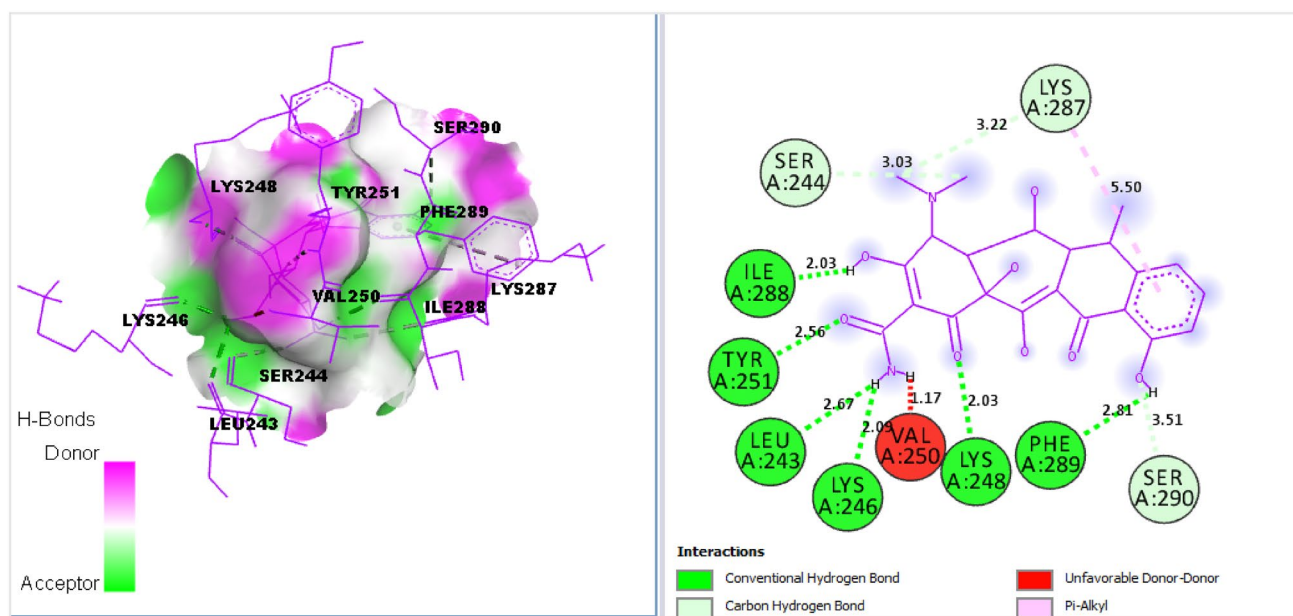
Fig. 5 Binding interaction between **doxycycline** and Cytoplasmic incompatibility factor CidA (PDB: 7ESX)

not be orally bio-available when it has Hydrogen Bond Donors (HBD) of greater than 5, Hydrogen Bond Acceptors (HBA) > 10, Molecular Weight (MW) > 500, and lipophilicity (MLOGP > 4.15 or WLOGP > 5) (Lipinski et al. 2001). Whenever a molecule passed at least three of the four provisions of the RO5, it is said to comply with Lipinski's rule for oral bioavailability (Lawal et al. 2021). Table 5 showed that all the tested pyrazolopyrimidine derivatives passed the drug-likeness test (Lipinski RO5) by showing no violation. The reported values of Topological Polar Surface Area (TPSA) for the molecules were less than 140 $Å^2$. Also, the values of the synthetic accessibility (SA) scores of these compounds were less than 5.00 (easy portion on a scale of 1–10), suggesting easy laboratory synthesis. The predicted values of the estimated water solubility (Log S) are in the range of $-4 > Log S > -6$, indicating these molecules are moderately soluble. The compounds were equally estimated to be free from pains and brenk alerts.

The estimated ADMET properties reported in Table 6, showed a very high Human Intestinal Absorption (HIA) (greater than 90%) for all tested compounds. Skin permeability is a key factor in transdermal drug delivery development. Values of skin permeation constant LogKp > − 2.50 indicates poor skin permeability. As a result, the various compounds tested showed LogKp values < − 2.50, connoting good skin permeability. Drug molecule penetration through the Blood-Brain Barrier (BBB) and Central Nervous System (CNS) comes with certain criteria. To enable a drug molecule penetrates the BBB and CNS readily, the logarithmic ratio of brain to plasma drug concentration (logBB) must be > 0.3 and the blood-brain permeability-surface area product (logPS) be > − 2 respectively. Consequently, only **14** with logBB of 0.325 readily penetrate the BBB as also indicated by its location within the boiled egg's yolk shown in Fig. 6, while the various compounds are non-CNS permeable. Also, **23**, **26**, and **29** were located in the Boiled Egg's white, an indication that they were predicted to be passively absorbed by the gastrointestinal tract.

Table 5 Predicted drug-likeness properties of some selected pyrazolopyrimidine derivatives

Comp ID	MW (g/mol)	TPSA ($Å^2$)	MLOGP	Log S (ESOL)	HBD	HBA	RO5	PAINS	BRENK	SA
14	359.40	55.11	3.56	− 4.60	1	4	0	0	0	3.28
23	387.43	81.41	2.79	− 4.49	1	5	0	0	0	3.26
26	437.54	72.93	3.26	− 5.47	1	4	0	0	0	3.67
29	442.51	84.65	2.23	− 4.28	1	5	0	0	0	3.58

MW molecular weight, *TPSA* topological polar surface area, *ESOL* estimated solubility, *HBD* hydrogen bond donors, *HBA* hydrogen bond acceptors, *RO5* Lipinski rule of five violation, *SA* synthetic accessibility score

Table 6 Predicted ADMET properties of some selected pyrazolopyrimidine derivatives

Comp ID	Absorption HIA (%)	Skin LogKp	Distribution BBB LogBB	CNS LogPS	Metabolism CYP34A S	CYP34A I	CYP2D6 S	CYP2D6 I	Excretion Total clearance	Toxicity AMES	MRTD
14	95.55	− 2.74	0.325	− 2.060	YES	YES	NO	NO	0.246	YES	− 0.253
23	98.01	− 2.74	− 0.801	− 2.439	YES	YES	NO	NO	0.701	NO	− 0.087
26	98.62	− 2.73	− 0.804	− 2.022	YES	YES	NO	NO	0.791	NO	0.172
29	96.12	− 2.75	− 0.146	− 2.953	YES	YES	NO	NO	0.591	NO	0.147

BBB Blood brain barrier, *CNS* Central nervous system, *HIA* Human intestinal absorption, *Skin* skin permeability, *LogBB* the logarithmic ratio of brain to plasma drug concentration, *LogPS* blood-brain permeability-surface area product, *CYP34A/CYP2D6* cytochrome p450 isoforms, *S* substrate, *I* inhibitor, *MRTD* Maximum recommended tolerated dose

Furthermore, some group of enzymes called cytochrome P450 enzymes are important in the body to facilitate drug metabolism and to help in their excretion. The two major isoforms enhancing drug metabolism, CYP-34 A and CYP-2D6 were tested. The tested molecules are not substrates and inhibitors of CYP2D6 but are both substrates and inhibitors of CYP3A4, an indication of a well-moderated metabolic process. Figure 6 showed that only compound **23** was predicted not to be effluated from the central nervous system by P-glycoprotein. P-glycoprotein acts as a biological barrier by extruding toxins and xenobiotics, including drugs out of cells. The extent of drug removal from the body is determined by the drug's total clearance. The range of values of total clearance for all the tested molecules is good. Additionally, all the compounds except **14** showed no AMES toxicity, implying that they are non-mutagenic and cannot act as carcinogens. Also available in Table 5 is the Maximum Recommended Tolerated Dose (MRTD) predicted for the various molecules. MRTD value of ≤ 0.477 log (mg/kg/day) is considered low, while a value > 0.477 log (mg/kg/day) is considered high. The overall drug-likeness and ADMET properties of the selected compounds showed good pharmacokinetic profiles, except compound **14** which showed positive AMES toxicity. Therefore, these molecules could be considered potential drug candidates for the treatment of filarial diseases.

Molecular dynamics simulation

To analyze the dynamics of the protein-ligand interaction, MD simulation was performed on the best protein-ligand interaction pair (**23_7ESX** complex) for 1ns (1000 ps) of chemical time (500,000 iterations). The results of this simulation as plots of Root-Mean-Square Deviation (RMSD), Root-Mean-Square Fluctuation (RMSF), Solvent Accessible Surface Area (SASA), and Radius of gyration (Rg) versus the time in ps were presented in Figs. 7, 8 and 9, and 10 respectively.

The average RMSD value was estimated as 1.6801 Å which showed that the protein-ligand complex deviated only a little from its original conformation during the trajectory. The deviation was maximum during the first 100ps of the simulation, after which it drops and tends to remain slightly unstable until a further drastic drop in the RMSD at 1000 ps, an indication that the system was fast attaining stability and nearing equilibrium (Edache et al. 2020). RMSF is more like a calculation of the flexibility or the extent of movement of individual residue during a simulation. As seen from Fig. 8, the RMSF tends to drop as the simulation nears 1000ps, a further indication that the system was fast attaining stability. The SASA is simply the surface area that is in contact with the solvent in which the complex resides. From Fig. 9, it can be observed that the SASA only fluctuates slightly between
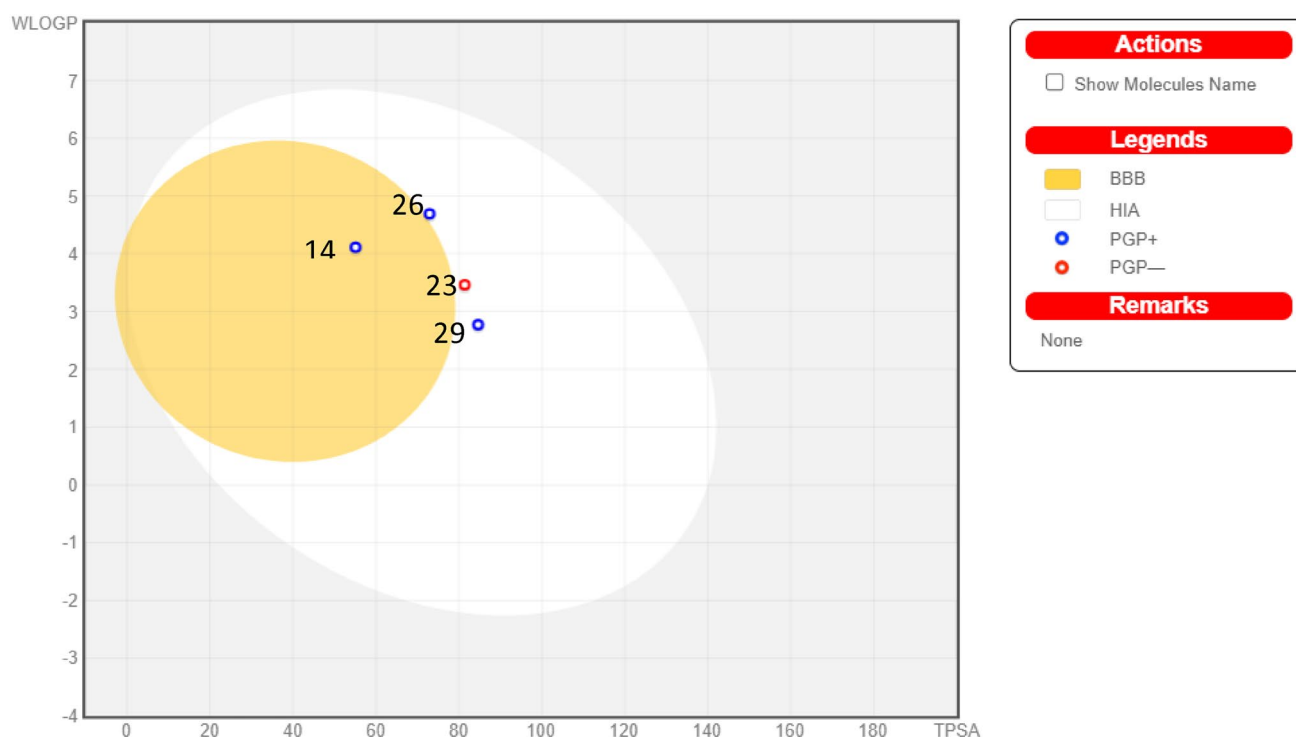
Fig. 6 The boiled-egg representation of compounds **14**, **23**, **26**, and **29**

10.50 Å^2 and 11.6 Å^2 during the trajectory, an indication of stability (Edache et al. 2022). The Rg is the measure of the degree of compactness of a protein during the trajectory. Decreasing Rg indicates reducing residues' flexibilities and more stability for the protein. Throughout the trajectory, the Rg varies between 27.283 Å and 28.365 Å which is equivalent to a difference of approximately 1.0 Å for the complex studied, connoting slight changes in the protein compactness as the simulation progresses, and therefore means the stability of the complex. Furthermore, it will not be complete without inspecting the simulated complex for possible

protein-ligand interactions. As a result, the simulated complex was visualized using the Biovia discovery studio and the resulting binding interaction of **23** with the active site of 7ESX is presented in Fig. 11.

The binding interaction pattern of the simulated complex (Fig. 11) deviated significantly from that of the non-simulated complex (Fig. 1) as several interactions majorly the hydrophobic interactions, electrostatic, and π-donor H-bond were lost. However, a significant number of important interactions were visible including Two (2) conventional H-bonding with SER-187 and ASN-77 at interaction distances of 2.32 Å and 1.94 Å respectively, Two (2) carbon H-bonding
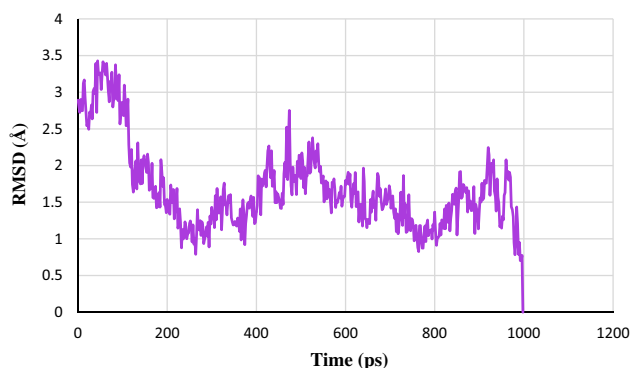

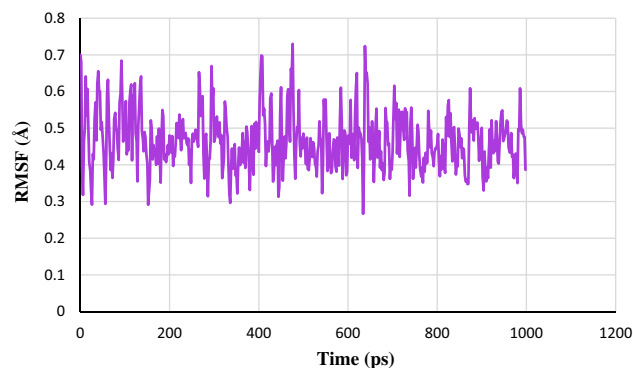**Fig. 7** The plot of RMSD versus time for MD simulation of **23** with 7ESX

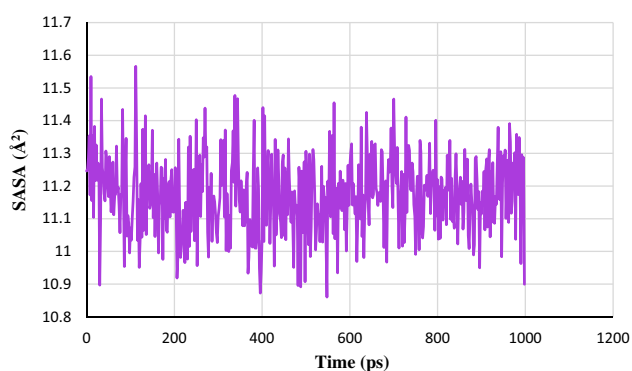**Fig. 8** The plot of RMSF versus time for MD simulation of **23** with 7ESX

Fig. 9 The plot of SASA versus time for MD simulation of **23** with 7ESX
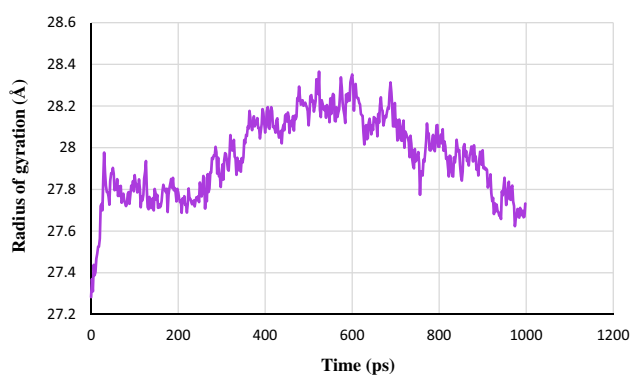

Fig. 10 The plot of radius of gyration versus time for MD simulation of **23** with 7ESX

with ASN-77 and LEU-75 at 2.96 Å and 2.75 Å respectively. Others are hydrophobic interactions with ARG-36 and ARG-74 at 4.12 Å and 4.66 Å respectively. Additionally, no unfavorable steric bumps or clashes were visible. Furthermore, the result of binding free energy (MM/GBSA) computed for **23_7ESX** by MolAICal is shown in Table 7.

The negative value of the estimated binding free energy (MM/GBSA) of the complex (− 60.6552 kcal/mol) indicates the favorability of the ligand-protein binding. Also, Van der Waals energy (− 50.0611 kcal/mol) contributed most to the binding free energy of the complex, connoting that Vander Waal/hydrophobic interactions played a crucial role in the binding process (Xu et al. 2019). It can therefore be inferred that compound **23** binds readily with the Cytoplasmic incompatibility factor CidA even within a dynamically perturbed system, and hence could be considered as a potential drug candidate for the treatment of filariasis.

3 – D QSAR modeling

Molecular structural alignment represents a key factor in ascertaining the predictive strength of a built 3-D QSAR model. Figure 12 (a–b) shows the molecular structure of the alignment template (compound **30**) and the aligned structures as obtained from the super-imposition of the remaining 51 molecules on the template. The UVEPLS approach was used to develop the model. Some significant statistical parameters calculated for the model were presented in Table 8. Reported in Table 9 were the experimental pEC_{50}, predicted pEC_{50}, and their residuals together with their O3A
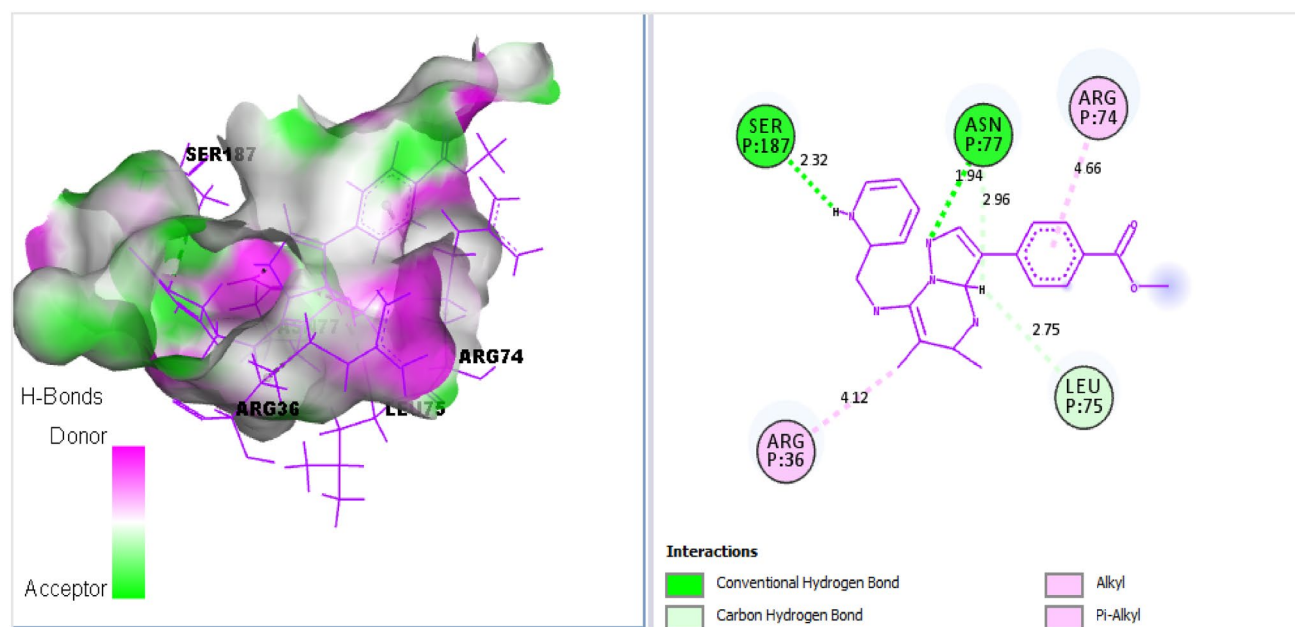

Fig. 11 Binding interaction between **23** and Cytoplasmic incompatibility factor CidA (PDB: 7ESX) after MD simulation
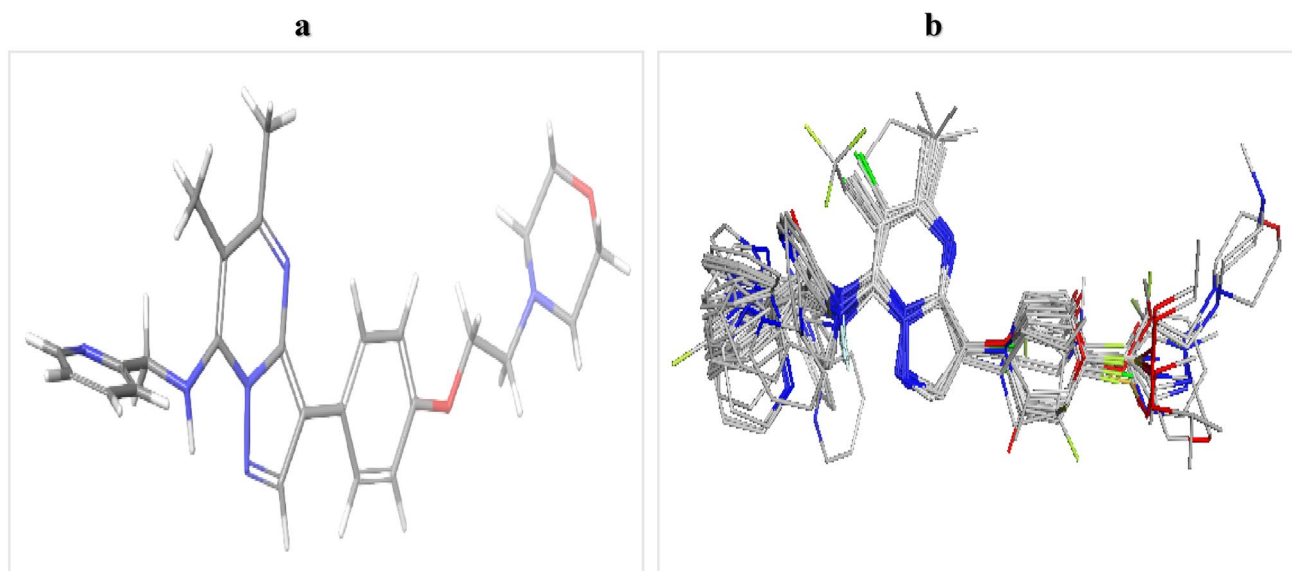
Fig. 12 Molecular alignment of structures for the QSAR modeling **a** Alignment template (compound **30** with the highest O3A_Score of 9057.78); **b** All structures aligned

scores. Additionally, a plot showing the correlation between predicted and experimental activities for both training and test sets was obtained and presented in Fig. 13. Also, the CoMFA model equation was summarized graphically as 3D contour maps as shown in Figs. 14 (a–b) and 15 (a–b).

The alignment process involves an early step that provided all the 52 compounds the opportunity of being chosen as the alignment template based on the compound with the highest Open3DAlign (O3A) score. The O3A scores of the various compounds were included in Table 8. Compound **30** had the highest O3A score of 9057.78 and hence was selected as the template upon which the remaining structures were superimposed. The model's statistical parameters were computed for Five (5) Principal Components (PC) amongst which the fifth PC (PC = 5) performed
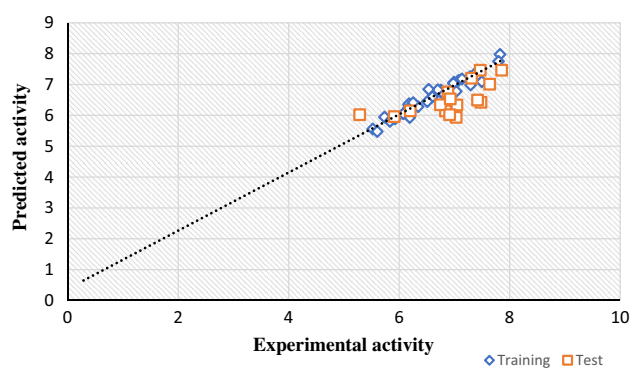
Table 7 Binding free energy parameters of 23_7ESX complex

Parameter	Value (kcal/mol)
ΔE(internal)	+ 15.1432
ΔE(electrostatic) + ΔG(solvation)	− 25.7373
ΔE (Van der Waal)	− 50.0611
ΔG binding (MM/GBSA)	− 60.6552 ± 0.528

relatively better with R^2 value of 0.9425, SDEC = 0.1446, and F-test = 98.282. The statistical parameters available in Table 9 were those associated with PC 5. The predictive strength of the regression models on new datasets of compounds can be estimated by cross-validation (Grohmann and Schindler 2008). A cross-validated coefficient of correlation $(Q^2) \geq 0.50$ indicates a good QSAR model. Here, three (3) types of Q^2 were calculated; Leave-one-out (LOO), Leave-two-out (LTO), and Leave-many-out (LMO), together with their associated Standard Error of Prediction (SDEP). Only Q^2_{LOO} (0.5019) passed this criterion and was reported alone.

A linear correlation between the CoMFA descriptors (independent variables) and the activity values (dependent variables) was established by the PLS analysis method. The lower residual values between the predicted and observed activity values (Table 8) shows a strong predictive strength of the model. This was supported by the clustering of points along the lines of best fit in the plots of predicted pEC_{50}
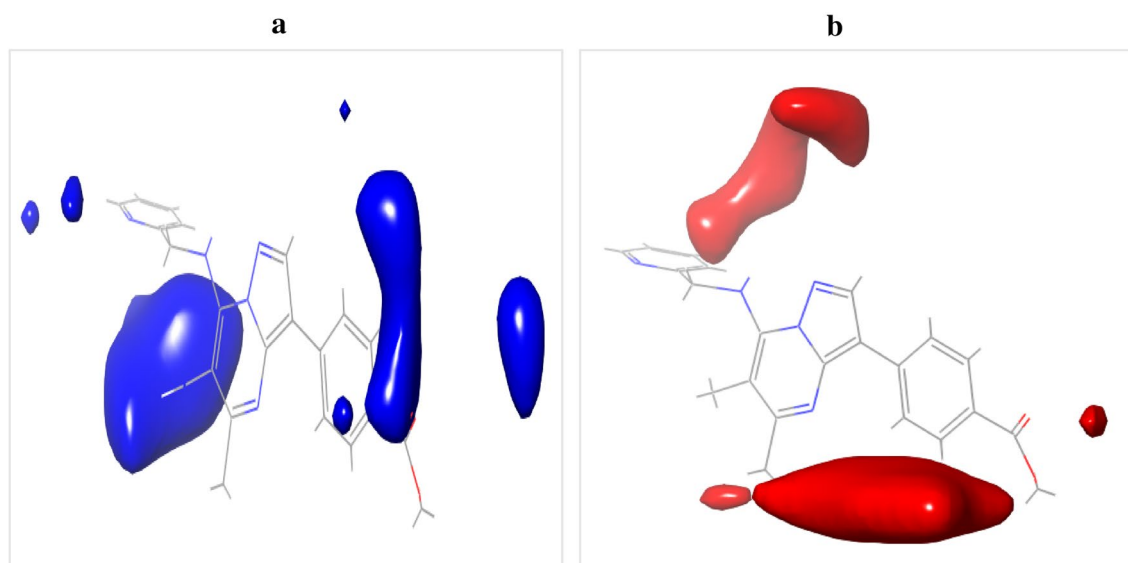

Fig. 13 Correlation between predicted and experimental pEC_{50} for training and test sets

Fig. 14 Steric field contour maps of compound **23 a** Blue contours represent regions of favorable steric bulk; **b** Red contours showing regions of unfavorable steric bulk

versus the experimental pEC_{50} (Fig. 13). This observation was supported by the conformation of the model to the Golbraikh and Tropsha criteria (Table 5) (Roy et al. 2016). The CoMFA QSAR equation is summarized graphically as a 3D

Table 8 Statistical parameters of the built model

Parameters		(UVEPLS)
PC		5
R^2		0.9425
SDEC		0.1446
F test		98.282
Q^2_{LOO}		0.5019
$SDEP_{LOO}$		0.4253
Golbraikh and Tropsha acceptable model criteria		
r^2	0.7501	$r^2 > 0.60$
$\left\|r_o^2 - r_o'^2\right\|$	0.1074	$\left\|r_o^2 - r_o'^2\right\| < 0.3$
$\left\|(r^2 - r_0^2)/r^2\right\|$	0.00123	$\left\|(r^2 - r_0^2)/r^2\right\| < 0.1$
k	1.0457	$0.85 < k < 1.15$
Field contributions		
Steric		0.5093 (50.93%)
Electrostatic		0.4907 (49.07%)

PC principal components, *SDEP* standard error of prediction, *F test* Fischer's statistics, *LOO* leave one out, Q^2 cross-validated correlation coefficient, R^2 Correlation coefficient, *SDEC* standard error of a correlation, *k* slope of the plot of predicted activity against experimental activity, r^2 square correlation coefficients of the plot of experimental activity versus predicted activity values, r_o^2 square correlation coefficients of the plot of experimental activity versus predicted activity values at zero intercept, $r_o'^2$ square correlation coefficients of the plot of predicted activity versus experimental activity at zero intercept

contour map, which shows the regions within the molecules' 3-D structural space where steric and electrostatic fields are associated with extreme values. The underlying principle behind CoMFA is that variations in the shape and strength of non-covalent interaction fields surrounding the molecules, such as steric or electrostatic fields can be related to changes in binding affinities (Kakarla et al. 2016). Therefore, molecular fields are key factors in binding affinity. The steric and electrostatic field contributions were 50.93% and 49.07% respectively (Table 9).

From the steric field contour maps available in Fig. 14 (a–b), the red contours represent regions of unfavorable steric bulk, while the blue contours show regions of favorable steric bulk. Regions in which steric bulk may reduce activity or affinity of the compound include positions 3 and 4 on the pyridine group, position 5 on the pyrimidine group, and position 2 on the benzoate group (Fig. 14b). For example, substituting the methyl group on position 5 of the pyrimidine group with a more bulky group like ethyl, isopropyl or tert-butyl could reduce the activity or binding affinity of the compound. On the other hand, more steric bulk favorable regions were identified (Fig. 14a), which include position 6 in the pyrimidine group, position 6 in the pyridine group, and position 2 in the benzoate group. This implies that the introduction of bulky substituent groups at these positions will improve the inhibitory activity of the molecule. From the electrostatic field contour maps available in Fig. 15(a–b), yellow contours represent regions favored by high electron density or unfavorable to electron-withdrawing substituents, while the green contours represent regions of unfavorable high electron density or favorable to electron-withdrawing
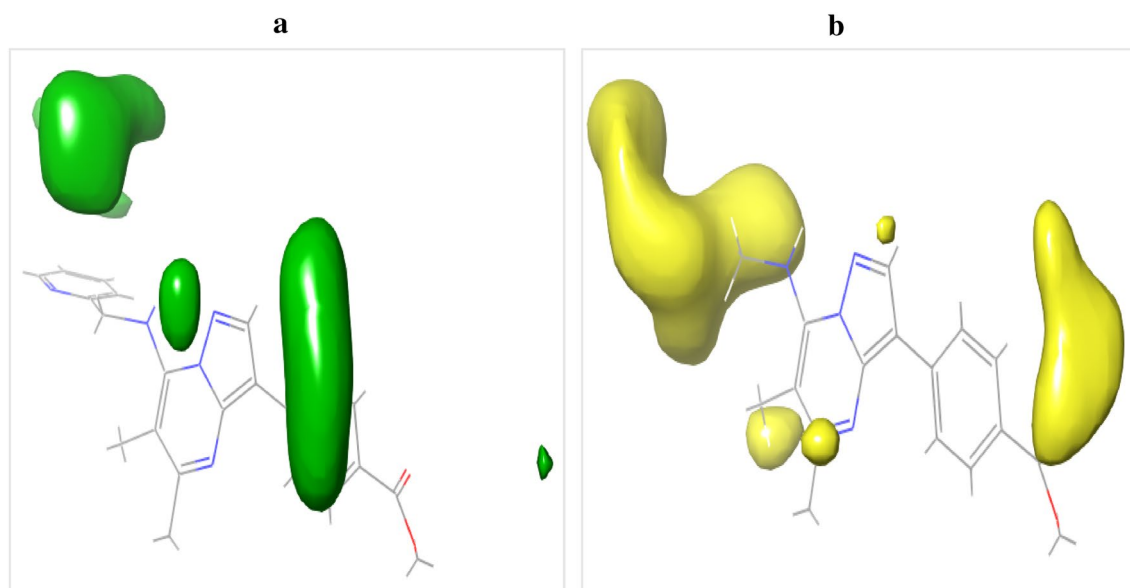
a   **b**

Fig. 15 Electrostatic field contour maps of compound **23 a** Green contours showing regions of unfavorable high electron density or favorable to electron-withdrawing groups; **b** Yellow contours repre-sent regions favored by high electron density or unfavorable to electron-withdrawing substituents

groups. Five (5) regions in which the introduction of electron-withdrawing groups could reduce the inhibitory activity or binding affinity include all positions in the pyridine group, positions 5 and 6 in the pyrimidine group, position 2 in the pyrazole group, and the carbonyl group of the benzoate moiety (Fig. 15b). Also, regions of unfavorable high electron density were visible around the benzene ring system of the benzoate group and between the linker amine group and the pyrazole hetero atom. These regions need not be too electron-dense, hence electron-withdrawing groups will keep these regions at a low electron density which in turn will enhance the molecule's inhibitory activity or binding affinity. In general, contour map analysis serves as a guide to designing new molecules with improved potency by adhering to the information encoded in the contour maps.

Conclusion

In this study, a molecular docking-based virtual screening, pharmacokinetics analysis, molecular dynamic simulation, and 3-D QSAR modeling were performed on the pyrazolopyrimidine derivatives. The molecular docking screening was effective as the Five (5) best protein-ligand interaction pairs were identified and ranked as 23_7ESX (– 10.2 kcal/mol) > 14_6EEZ (– 9.0 kcal/mol) > 29_3F4R (– 8.0 kcal/mol) > 26_6W9O (– 7.7 kcal/mol) $\approx$ doxycycline_7ESX (– 7.7 kcal/mol). The selected analogs (**14**, **23**, **26**, and **29**) all obeyed Lipinski's RO5 for oral bio-availability and showed excellent ADMET properties except **14**, with positive AMES toxicity. Results of the MD simulation showed the stability of the 23_7ESX complex, exhibiting a favorable ligand-protein binding process with an estimated ΔG binding (MM/GBSA) of – 60.6552 kcal/mol. The 3 – D QSAR (CoMFA) model was developed and found to satisfy the requirement for validation tests with R^2 value of 0.9425, $Q^2_{LOO} = 0.5019$, SDEC = 0.1446, and F test = 98.282. The anti-*Wolbachia* activities of the various compounds were well predicted by the model. The analysis of the steric and electrostatic contour maps could provide a useful guide for the future design of more active analogs. Special emphasis on compound **23** because it appears to be consistent with the various employed validation protocols, being that it possessed the highest binding score, showed excellent pharmacokinetic properties, and binds pharmacologically well with the target protein (7ESX). Therefore, **23** could be considered as a potential filarial drug candidate, and/or template for the design of more prominent *Wolbachia* inhibitors.

Table 9 Observed pEC$_{50}$, predicted pEC$_{50}$, residuals, and Open3DAlign scores of the various pyrazolopyrimidine derivatives

Comp ID	EC$_{50}$ (nM)	pEC$_{50}$	Pred. pEC$_{50}$	Residuals	O3A Score
1	647	6.189	5.934	0.255	8591.09
2	1854	5.732	5.946	− 0.214	8602.81
3	3012	5.521	5.562	− 0.041	8306.61
4*	5176	5.286	6.022	− 0.736	8231.71
5	1384	5.859	5.865	− 0.006	8554.70
6*	145	6.839	6.146	0.693	8567.27
7*	90	7.046	6.338	0.708	7866.65
8*	93	7.032	5.936	1.096	8524.64
9*	33	7.481	6.426	1.055	8346.95
10	183	6.737	6.782	− 0.045	8389.24
11	518	6.286	6.286	0.00	8865.76
12	456	6.341	6.282	0.059	8561.81
13	2500	5.602	5.481	0.121	8035.49
14	93	7.032	6.782	0.25	8992.31
15	51	7.292	6.986	0.306	8755.17
16	15	7.824	7.98	− 0.156	8571.70
17	674	6.171	6.35	− 0.179	8757.04
18	664	6.178	6.178	0.00	8998.60
19	143	6.845	6.747	0.098	8895.54
20	664	6.178	6.382	− 0.204	8888.54
21	84	7.076	7.139	− 0.063	8551.79
22	102	6.991	7.082	− 0.091	8161.13
23*	179	6.747	6.346	0.401	8923.84
24	175	6.757	6.764	− 0.007	8943.94
25*	131	6.883	6.762	0.121	8918.56
26	1479	5.83	5.808	0.022	9053.70
27*	119	6.925	6.538	0.387	8743.78
28	43	7.367	7.351	0.016	7901.16
29	680	6.167	6.233	− 0.066	9022.08
30	844	6.074	6.055	0.019	9057.78
31*	1228	5.911	5.961	− 0.05	8789.76
32	105	6.979	7.041	− 0.062	6769.31
33	176	6.754	6.823	− 0.069	6961.39
34*	122	6.914	6.025	0.889	6443.42
35	164	6.785	6.731	0.054	7026.31
36	251	6.6	6.602	− 0.002	6816.61
37*	629	6.201	6.148	0.053	6770.61

Table 9 (continued)

Comp ID	EC$_{50}$ (nM)	pEC$_{50}$	Pred. pEC$_{50}$	Residuals	O3A Score
38	311	6.507	6.449	0.058	7194.85
39	52	7.284	7.259	0.025	7723.79
40	73	7.137	7.186	−0.049	7960.74
41	561	6.251	6.414	−0.163	8114.80
42*	38	7.42	6.499	0.921	7833.08
43	16	7.796	7.752	0.044	8375.87
44	1183	5.927	5.892	0.035	7708.13
45	201	6.697	6.831	−0.134	6377.11
46	38	7.42	7.313	0.107	7915.01
47	293	6.533	6.85	−0.317	8661.85
48	32	7.495	7.094	0.401	7986.54
49*	14	7.854	7.465	0.389	7198.67
50*	23	7.638	7.013	0.625	6738.02
51*	34	7.468	7.465	0.003	7198.68
52*	49	7.31	7.206	0.104	7380.57

*Test set compounds

Data availability All data related to this study are included herein otherwise available on request.

Declarations

Conflict of interest The authors declare that they have no competing interests.

Ethical approval and consent to participate Not applicable.

Consent for publication Not applicable.

References

Adeniji SE, Arthur DE, Abdullahi M, Abdullahi A, Ugbe FA (2020) Computer-aided modeling of triazole analogues, docking studies of the compounds on DNA gyrase enzyme and design of new hypothetical compounds with efficient activities. Journal of Biomolecular Structure and Dynamics. https://doi.org/10.1080/07391102.2020.1852963

Al-Attraqchi OH, Mordi MN (2022) 2D- and 3D-QSAR, molecular docking, and virtual screening of pyrido [2, 3-d] pyrimidin-7-one-based CDK4 inhibitors. J Appl Pharm Sci 12(01):165–175

Bai Q, Tan S, Xu T, Liu H, Huang J, Yao X (2020) MolAICal: a soft tool for 3D drug design of protein targets by artificial intelligence and classical algorithm. Brief Bioinform 00(00):1–12. doi:https://doi.org/10.1093/bib/bbaa161

Bakowski MA, Shiroodi RK, Liu R, Olejniczak J, Yang B, Gagaring K, Guo H, White PM, Chappell L, Debec A, Landmann F, Dubben B, Lenz F, Struever D, Ehrens A, Frohberger SJ, Sjoberg H, Pionnier N, Murphy E, Archer J, Steven A, Chunda VC, Fombad FF, Chounna PW, Njouendou AJ, Metuge HM, Ndzeshang BL, Gandjui NV, Akumtoh DN, Kwenti TDB, Woods AK, Joseph SB, Hull MV, Xiong W, Kuhen KL, Taylor MJ, Wanji S, Turner JD, Hübner MP, Hoerauf A, Chatterjee AK, Roland J, Tremblay MS, Schultz PG, Sullivan W, Chu XJ, Petrassi HM, McNamara CW (2019) Discovery of short-course antiwolbachial quinazolines for elimination of filarial worm infections. Sci Transl Med 11(491):87. https://doi.org/10.1126/scitranslmed.aav3523

Bouchery T, Lefoulon E, Karadjian G, Nieguitsila A, Martin C (2013) The symbiotic role of Wolbachia in Onchocercidae and its impact on filariasis. Clin Microbiol Infect 19(2):131–140

Carter DS, Jacobs RT, Freund Y, Berry P, Akama T, Easom EE, Lunde CS, Rock FL, Stefanakis R, McKerrow JH, Fischer C, Bulman C, Lim KC, Suzuki BM, Tricoche N, Sakanari J, Lustigman S, Plattner JJ (2020) Macrofilaricidal benzimidazole-benzoxaborole hybrids as an approach to the treatment of river blindness, part 2: ketone linked analogs. ACS Infect Dis 6(2):180–185

Edache EI, Uzairu A, Mamza PA, Shallangwa GA (2020) A comparative QSAR analysis, 3D- QSAR, molecular docking and molecular design of iminoguanidine-based inhibitors of HemO: A rational approach to antibacterial drug design. Journal of Drugs and Pharmaceutical Science. https://doi.org/10.31248/JDPS2020.036

Edache EI, Uzairu A, Mamza PA, Shallangwa GA (2022) Computational modeling and analysis of the theoretical structure of thiazolino 2pyridone amide inhibitors for Yersinia pseudotuberculosis and Chlamydia trachomatis Infectivity. Bull Sci Res 4(1):14–39

ElMchichi L, Belhassan A, Lakhlifi A, Bouachrine M (2020) 3D-QSAR study of the chalcone derivatives as anticancer agents. Hindawi Journal of Chemistry. https://doi.org/10.1155/2020/5268985

Grohmann R, Schindler T (2008) Toward robust QSPR models: Synergistic utilization of robust regression and variable elimination. J Comput Chem 29(6):847–860

Ibrahim MT, Uzairu A, Shallangwa GA, Uba S (2020) Lead identification of some anti-cancer agents with prominent activity against Non-small Cell Lung Cancer (NSCLC) and structure-based design. Chem Afr 3:1023–1044

Ibrahim MT, Uzairu A, Uba S, Shallangwa GA (2021) Design of more potent quinazoline derivatives as EGFRWT inhibitors for the treatment of NSCLC: a computational approach. J Pharm Sci 7:140

Jacobs RT, Lunde CS, Freund YR, Hernandez V, Li X, Xia Y, Carter DS, Berry PW, Halladay J, Rock F, Stefanakis R, Easom E, Plattner JJ, Ford L, Johnston KL, Cook DAN, Clare R, Cassidy A, Myhill L, Tyrer H, Gamble J, Guimaraes AF, Steven A, Lenz F, Ehrens A, Frohberger SJ, Koschel M, Hoerauf A, Hübner MP, McNamara CW, Bakowski MA, Turner JD, Taylor MJ, Ward SA (2019) Boron-Pleuromutilins as anti-wolbachia agents with potential for treatment of *onchocerciasis* and *lymphatic filariasis*. J Med Chem 62:2521–2540

Kakarla P, Inupakutika M, Devireddy AR, Gunda SK, Willmon TM, Ranjana KC, Shrestha U, Ranaweera I, Hernandez AJ, Barr S, Varela MF (2016) 3D-QSAR and contour map analysis of tariquidar analogues as Multidrug Resistance Protein-1 (MRP-1) inhibitors. Int J Pharm Sci Res 7(2):554–572

Kumar NA, Sharmila R, Akila K, Jaikumar B (2016) In-silico approach for the assessment of oral cancer property on limonia acidissima. IJPSR 7(3):1271–1275

Lakshmi V, Joseph SK, Srivastava S, Verma SK, Sahoo MK, Dube V, Mishra SK, Murthy PK (2010) Antifilarial activity in vitro and in vivo of some flavonoids tested against *Brugia malayi*. Acta Trop 116:127–133

Lawal HA, Uzairu A, Uba S (2021) QSAR, molecular docking studies, ligand-based design and pharmacokinetic analysis on Maternal Embryonic Leucine Zipper Kinase (MELK) inhibitors as potential anti-triple-negative breast cancer (MDA-MB-231cell line) drug compounds. Bulletin of the National Research Centre. https://doi.org/10.1186/s42269-021-00541-x

Lee J, Cheng X, Swails JM, Yeom MS, Eastman PK, Lemkul JA, Wei S, Buckner J, Jeong JC, Qi Y, Jo S, Pande VS, Case DA, Brooks CL, MacKerell AD Jr, Klauda JB, Im M (2016) CHARMM-GUI input generator for NAMD, GROMACS, AMBER, OpenMM, and CHARMM/OpenMM simulations using the CHARMM36 additive force field. J Chem Theory Comput 12:405–413

Lipinski CA, Lombardo F, Dominy BW, Feeney PJ (2001) Experimental and computational approaches to estimate solubility and permeability in drug discovery and development settings. Adv Drug Deliv Rev 46:3–26

McGillan P (2017) Development of small-molecule anti-*wolbachia* agents for the treatment of filariasis, PhD Thesis University of Liverpool. Retrieved from https://livrepository.liverpool.ac.uk/3016953. Accessed 24 Feb 2021

McGillan P, Berry NG, Nixon L, Leung SC, Webborn PJH, Wenlock MC, Kavanagh S, Cassidy A, Clare RH, Cook DA, Johnston KL, Ford L, Ward SA, Taylor MJ, Hong WD, O'Neill PM (2021) Development of pyrazolopyrimidine anti-*wolbachia* agents for the treatment of filariasis. ACS Med Chem Lett 12(9):1421–1426

Muniba F (2019) Tutorial: molecular dynamics (MD) simulation using Gromacs. Bioinform Rev 5(12). Retrieved from https://bioinformaticsreview.com/20191210/tutorial-molecular-dynamics-md-simulation-using-gromacs/. Accessed 22 Apr 2022

Roy K, Das RN, Ambure P, Aher RB (2016) Be aware of error measures. Further studies on validation of predictive QSAR models. Chemometr Intell Lab Syst 152:18–33

Sashidhara KV, Rao KB, Kushwaha V, Modukuri RK, Verma R, Murthy PK (2014) Synthesis and antifilarial activity of chalcone-thiazole derivatives against a human lymphatic filarial parasite, *Brugia malayi*. Eur J Med Chem 81:473–480

Sightsavers (2013) Policy brief: neglected tropical diseases. In sightsavers.org (2013) Retrieved from https://www.sightsavers.org/reports/2013/09/policy-neglected-tropical-diseases 2 May 2020

Slatko BE, Taylor MJ, Foster JM (2010) The *wolbachia* endosymbiont as an anti-filarial nematode target. Symbiosis 51(1):55–65

Tosco P, Balle T (2011) Open3DQSAR: a new open-source software aimed at high-throughput chemometric analysis of molecular interaction fields. J Mol Model 17(1):201–208

Ugbe FA, Shallangwa GA, Uzairu A, Abdulkadir I (2021) Activity modeling, molecular docking and pharmacokinetic studies of some boron-pleuromutilins as anti-wolbachia agents with potential for treatment of filarial diseases. Chem Data Collections 36:100783

Ugbe FA, Shallangwa GA, Uzairu A, Abdulkadir I (2022a) Theoretical modeling and design of some pyrazolopyrimidine derivatives as Wolbachia inhibitors, targeting lymphatic flariasis and onchocerciasis. Silico Pharmacol 10:8. https://doi.org/10.1007/s40203-022-00123-3

Ugbe FA, Shallangwa GA, Uzairu A, Abdulkadir I (2022b) Theoretical activity prediction, structure-based design, molecular docking and pharmacokinetic studies of some maleimides against Leishmania donovani for the treatment of leishmaniasis. Bull Natl Res Centre 46:92. https://doi.org/10.1186/s42269-022-00779-z

Wang X, Dong H, Qin Q (2020) QSAR models on aminopyrazole-substituted resorcylate compounds as Hsp90 inhibitors. J Comput Sci &Engineering 48:1146–1156

Xu Y, He Z, Yang M, Gao Y, Jin L, Wang M, Zheng Y, Lu X, Zhang S, Wang C, Zhao Z, Zhao J, Gao Q, Duan Y (2019) Investigating the binding mode of reversible LSD1 inhibitors derived from stilbene derivatives by 3D-QSAR, molecular docking, and molecular dynamics simulation. Molecules 24(24):4479. doi:https://doi.org/10.3390/molecules24244479

Zhang X, Yan J, Wang H, Wang Y, Wang J, Zhao D (2020) Molecular docking, 3D-QSAR, and molecular dynamics simulations of thieno [3, 2b] pyrrole derivatives against anticancer targets of KDM1A/LSD1. J Biomol Struct Dynamics. DOI: https://doi.org/10.1080/07391102.2020.1726819